Plasmon Coupling in Nanorod Assemblies: Optical Absorption, Discrete Dipole Approximation Simulation, and Exciton-Coupling Model

Prashant K. Jain, Susie Eustis, and Mostafa A. El-Sayed*

Laser Dynamics Laboratory, School of Chemistry and Biochemistry, Georgia Institute of Technology, Atlanta, Georgia 30332-0400

Received: June 21, 2006; In Final Form: August 2, 2006

The shape anisotropy of nanorods gives rise to two distinct orientational modes by which nanorods can be assembled, i.e., end-to-end and side-by-side, analogous to the well-known *H* and *J* aggregation in organic chromophores. Optical absorption spectra of gold nanorods have earlier been observed to show a red-shift of the longitudinal plasmon band for the end-to-end linkage of nanorods, resulting from the plasmon coupling between neighboring nanoparticles, similar to the assembly of gold nanospheres. We observe, however, that side-by-side linkage of nanorods in solution shows a blue-shift of the longitudinal plasmon band and a red-shift of the transverse plasmon band. Optical spectra calculated using the discrete dipole approximation method were used to simulate plasmon coupling in assembled nanorod dimers. The longitudinal plasmon band is found to shift to lower energies for end-to-end assembly, but a shift to higher energies is found for the side-by-side orientation, in agreement with the optical absorption experiments. The strength of plasmon coupling was seen to increase with decreasing internanorod distance and an increase in the number of interacting nanorods. For both side-by-side and end-to-end assemblies, the strength of the longitudinal plasmon coupling increases with increasing nanorod aspect ratio as a result of the increasing dipole moment of the longitudinal plasmon. For both the side-by-side and end-to-end orientation, the simulation of a dimer of nanorods having dissimilar aspect ratios showed a longitudinal plasmon resonance with both a blue-shifted and a red-shifted component, as a result of symmetry breaking. A similar result is observed for a pair of similar aspect ratio nanorods assembled in a nonparallel orientation. The internanorod plasmon coupling scheme concluded from the experimental results and simulations is found to be qualitatively consistent with the molecular exciton coupling theory, which has been used to describe the optical spectra of *H* and *J* aggregates of organic molecules. The coupled nanorod plasmons are also suggested to be electromagnetic analogues of molecular orbitals. Investigation of the plasmon coupling in assembled nanorods is important for the characterization of optical excitations and plasmon propagation in these nanostructures. The surface plasmon resonance shift resulting from nanorod assembly also offers a promising alternative for analyte-sensing assays.

I. Introduction

Recently, increasing amount of attention has been directed toward the assembly of metal nanoparticle building blocks into ordered structures[1−11] for biodiagnostic[1,2,8,11−16] and potential optoelectronic device applications[17−23] like photonic waveguiding[24−30] and optical switching.[31,32] The process of metal nanosphere assembly or aggregation is known to alter the optical properties of the nanostructure.[12,33−38] For instance, the nanosphere surface plasmon resonance shifts to lower energies in assembled structures, which is attributed to the electromagnetic coupling of plasmons of the individual nanospheres interacting in the assembly.[12,38,39] The Mirkin[16] and Alivisatos[11] groups have already demonstrated biosensing schemes based on the programmed assembly of gold and silver nanospheres using proteins and nucleic acids, a more recent example being the "molecular plasmon ruler" described by Sonnichsen et al.[40] There has been a strong interest in understanding plasmon coupling in assembled metal nanostructures; detailed investigations have been carried out by past experiments and computational electromagnetic simulations of metal nanosphere dimers,[39,41−43] chains,[29,36] and 2D[44] and 3D assemblies/aggregates.[35,38] Besides applications in surface plasmon resonance-based biosensing, interparticle electromagnetic coupling has been proposed to result in a strong localized enhancement of the electric field in the gap between the particles,[45,46] allowing enhanced Raman scattering,[47,48] photoluminescence,[49] multiphoton excitation,[50] and other linear and nonlinear spectroscopies[51,52] of adsorbed molecules. The Atwater[25−28] and Krenn groups[24,29] have also demonstrated the utility of the near-field plasmon coupling between assembled metal nanospheres for photonic waveguiding below the diffraction limit.

On account of their anisotropic structure, gold nanorods possess much more interesting optical properties as compared to nanospheres,[3,53,54] including stronger and tunable absorption (corresponding to the longitudinal plasmon oscillation),[55−59] enhanced photoluminescence,[60,61] higher surface-enhanced Raman cross-sections,[62,63] and the possibility of unidirectional plasmon propagation,[64] thus motivating interest in the controlled assembly of nanorods into functional architectures as well as for analyte-sensing applications.[3,65] The Murphy group[66,67] and Nikoobakht et al.[68] have already demonstrated self-assembly of gold nanorods. On account of their shape anisotropy, nanorods can be assembled via two orientational modes.

* To whom correspondence should be addressed. E-mail: mostafa.el-sayed@chemistry.gatech.edu; Tel: 404-894-0292; Fax: 404-894-0294.

10.1021/jp063879z CCC: $33.50
Published on Web 08/30/2006

Selective end-to-end functionalization and 1D assembly of gold nanorods has been achieved by the use of the streptavidin−biotin linkage,[69,70] thiolated-DNA hybridization schemes[71] and co-operative hydrogen-bonding schemes based on thiolated molecules.[72] Recently, Kamat and co-workers[72] as well as Joseph et al.[73] used thioalkyl carboxylic acid-based bifunctional molecules for end-to-end alignment of nanorods in solution. They also demonstrated by optical spectroscopy that the end-to-end assembly process leads to a red-shift in the longitudinal plasmon resonance of the nanorod spectrum, similar to the case of nanosphere assembly.

In the present work, we explore the orientational dependence of plasmon coupling in assemblies of anisotropic plasmonic nanoparticles. We observed that the aggregation of gold nanorods in a side-by-side orientation in solution shows a blue-shift of the longitudinal nanorod plasmon band and a red-shift of the transverse band. The plasmon coupling in side-by-side vs end-to-end dimers of nanorods is systematically modeled by the discrete dipole approximation method, showing qualitative agreement with the experimental shifts in the optical resonance bands i.e., red-shift of the longitudinal plasmon band for end-to-end assembly in contrast to the blue-shift for the case of side-by-side assembly. For both end-to-end and side-by-side assembly, the strength of plasmon coupling is found to increase with decreasing internanorod distance and an increase in the number of rods in the assembly. Nanorods with increasing aspect ratio show increasing strength of longitudinal plasmon coupling for both assembly orientations. Dimers of nanorods of dissimilar aspect ratio, rod-sphere pairs, as well as nanorods assembled in a nonparallel orientation are also investigated. The general scheme of plasmon coupling in assembled nanostructures as inferred from the experimental and simulation results is found to be qualitatively consistent with the exciton coupling model.[74,75] The situation of side-by-side vs end-to-end assembly of nanorods is thus found analogous to the *H* and *J* aggregation of organic molecules.[76]

II. Experimental Section

A. Experimental Methods. Gold nanorods were prepared by the chemical seeding technique described previously.[61] Briefly, a seed solution was generated by adding ice cold $NaBH_4$ to a solution of $HAuCl_4$ and cetyltrimethylammonium bromide (CTAB). The solution was kept at 25 °C for a few minutes before use. A brownish-yellow color was observed in all seed solutions used. The growth solution contained 5 mL of a solution of 0.20 mM CTAB and 0.25 mM benzyldimethylammonioum chloride hydrate (BDAC), which was added to 0.20 mL of 4.0 mM $AgNO_3$. Then 5.0 mL of 0.90 mM $HAuCl_4$ and 54 μL of 0.10 M ascorbic acid were added. Twelve milliliters of seed solution was then added to the solution, which was left undisturbed for 4 h for the nanorods to grow. Kinetic growth conditions determine the aspect ratio of the nanorods generated, with narrower widths in the higher aspect ratio samples. Optical extinction spectra of the synthesized nanorods were recorded on a UV−Vis−NIR scanning spectrometer. The nanorod samples were imaged on a JEOL100 transmission electron microscope (TEM). The gold nanorods have a positively charged surface due to the presence of adsorbed CTA^+ ions and the aggregation of nanorods in solution was induced by the addition of 0.07 M sodium citrate solution to 1 mL of the nanorod solution and monitored by UV−Vis optical extinction. Resulting nanorod aggregates were imaged by TEM by drop casting the aggregated nanorod solution onto a copper grid placed on a filter paper and allowed to dry.

B. Calculation Methods. To model the plasmon coupling in the assembled nanorod structures, optical spectra of isolated nanorods, nanorod dimers, and nanorod trimers were calculated by the discrete dipole approximation (DDA) method—a discretization procedure for solving the Maxwell's equations where the target particle is geometrically reproduced by a cubic array of virtual point dipoles. DDA has been demonstrated to be one of the most powerful and flexible electrodynamic methods for computing the optical spectra of particles with an arbitrary geometry. Details of the DDA method have been described elsewhere.[77] The Schatz group[78,79] has already carried out extensive studies showing that DDA is suited for optical calculations of the extinction spectrum and the local electric field distribution in metal particles with different geometries and environments. Recently, Pileni and co-workers have established the applicability of using DDA simulations to model experimental optical spectra of gold nanorods.[80] Using the DDA method, Lee and El-Sayed have investigated the systematic dependence of nanorod absorption and scattering on their aspect ratio, size, and medium refractive index.[81]

The spectra of the extinction efficiency of nanorods and assembled nanorod structures were calculated by employing the DDSCAT code developed by Draine and Flatau.[77] The nanorod shape was approximated by a cubic array ($40 \times 10 \times 10$) of point dipoles representing a prolate spheroid. In DDSCAT, the size of the nonspherical target of volume V is expressed in terms of an effective radius, $r_{\text{eff}} = (3V/4\pi)^{1/3}$, which is the radius of a sphere having a volume equal to that of the particle. The nanorod target used for most of the calculations had $r_{\text{eff}} = 16$ nm and aspect ratio AR (i.e., the ratio of the long axis a to the short axis b of the particle) of 4.0, which is also equivalent to $a \approx 80$ nm and $b \approx 20$ nm. Calculations were carried also carried out for two other values of the nanorod aspect ratio, $AR = 2.8$ and 3.5 while the effective radius was kept constant. Dipole representations of assembled nanorod dimers (corresponding $r_{\text{eff}} = 20$ nm) and trimers (corresponding $r_{\text{eff}} = 23$ nm) in different orientations i.e., assembled side-by-side, end-to-end, or with their axes mutually perpendicular were generated. The center-to-center distance R between the interacting nanorods was also varied. Although a quasi-static treatment of the interaction between cylindrical particles (each represented by a single point dipole) has been undertaken earlier,[82] the DDA method does not place any dipolar limit on the center-to-center distance between the particles because each particle is modeled by a few thousand point-dipoles. The chief requirement for the applicability of DDA is that the interdipole separation d be small compared to any structural dimensions of the target and the wavelength of light λ, or, in other words, that a sufficient number of dipoles be employed to represent the target. This criterion is quantitatively expressed as $|n|kd < 1$, where n is the complex refractive index of the target material. Validity of this criterion was verified by the DDSCAT program. Note that the accuracy of the DDSCAT calculations can be increased by increasing the number of dipoles used to simulate the target, however with a significant increase in the computational cost especially for assembled nanostructures. The target particle in the surrounding dielectric medium is considered by using a dielectric function of the target ϵ relative to that of the medium ϵ_m, which is reflected in the DDA calculation in the form of a dipole polarizability. The dielectric function of gold was generated from the bulk experimental data of Johnson and Christy[83] and the medium was assumed to have a refractive index n_m of 1.33 corresponding to that of liquid water. Dipole polarizabilities were assigned by the lattice dispersion relation (LDR) developed

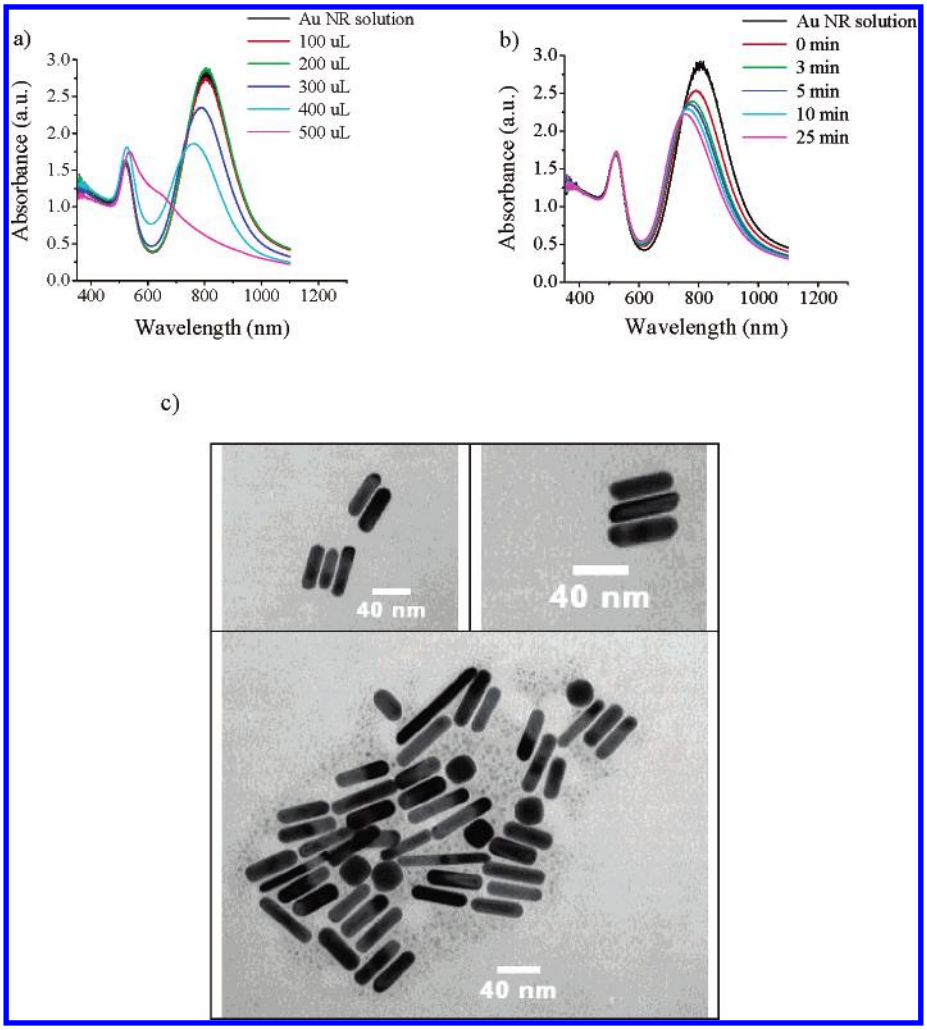

Figure 1. UV−visible extinction spectra of a 1-mL gold nanorod solution (shown in black) (a) on addition of increasing aliquots (100, 200, 300, 400, and 500 μL) of 0.07 M sodium citrate solution, and (b) on addition of 300 μL of 0.07 M sodium citrate solution at different time intervals (0, 3, 5, 10, and 25 min). (c) TEM images of a solution of gold nanorods aggregated by the addition of sodium citrate showing aggregation of nanorods in a side-by-side arrangement.

by Draine and Goodman,[84] which includes a radiative reaction correction term and is suited for finite dipole arrays. The light polarization direction E with respect to the nanorod assembly was selected so as to model the longitudinal plasmon excitation mode and the transverse mode separately.

III. Results and Discussion

Optical Absorption Changes. The visible extinction spectrum of the gold nanorod solution shows a wavelength maximum around 520 nm corresponding to the transverse plasmon oscillation band and a higher intensity maximum around 805 nm corresponding to the longitudinal plasmon oscillation.[59] An average aspect ratio of 3.2 was obtained for the nanorod sample by fitting the experimental extinction spectrum to Gans' theory as described elsewhere.[61,85] Figure 1a shows the evolution of the optical spectrum of the gold nanorod solution upon the addition of increasing aliquots of 0.07 M sodium citrate solution to 1 mL of the nanorod solution. Figure 1b shows the optical spectrum at different time intervals following addition of 300 μL of 0.07 M sodium citrate solution to the nanorod colloid. It is clearly seen that the addition of the sodium citrate induces the blue-shift of the longitudinal plasmon band along with a smaller red-shift of the transverse band. Visible color change of the solution from red to purple (with diminished color intensity) was also observed. These absorption changes are attributable to aggregation/assembly of the nanorods in solution induced by addition of sodium citrate, as also evidenced by the physical precipitation of metallic gold on further standing of the solution. It has been observed by Kamat and co-workers[72] and Joseph et al.[73] that the aggregation of gold nanorods induced by thiol carboxylic acid-based bifunctional linkers results in a red-shift of the longitudinal plasmon band without significant shift in the transverse plasmon band. These studies also established that thiol-based linker molecules selectively adsorb to the ends of the nanorods; further hydrogen bonding of the terminal carboxylic acid groups results in the end-to-end assembly of the nanorods. The optical band shifts in our nanorod aggregation experiments resulting from sodium citrate addition are clearly in contrast to those induced by the end-to-end assembly method. This contrast results possibly from the mechanism of nanorod assembly in our experiments, which we explore further.

Mechanism of Nanorod Assembly. A detailed study of the self-assembly of gold nanorods in the presence of carboxylate molecules has been carried out by the Murphy group.[66] In accordance with their proposed assembly mechanism, the gold nanorods in our experiments have a positively charged surface due to strongly adsorbed CTA^+ ions along the side surface. The resulting electrostatic repulsion between nanorods is responsible for the stability of the nanorods in solution. The colloidal

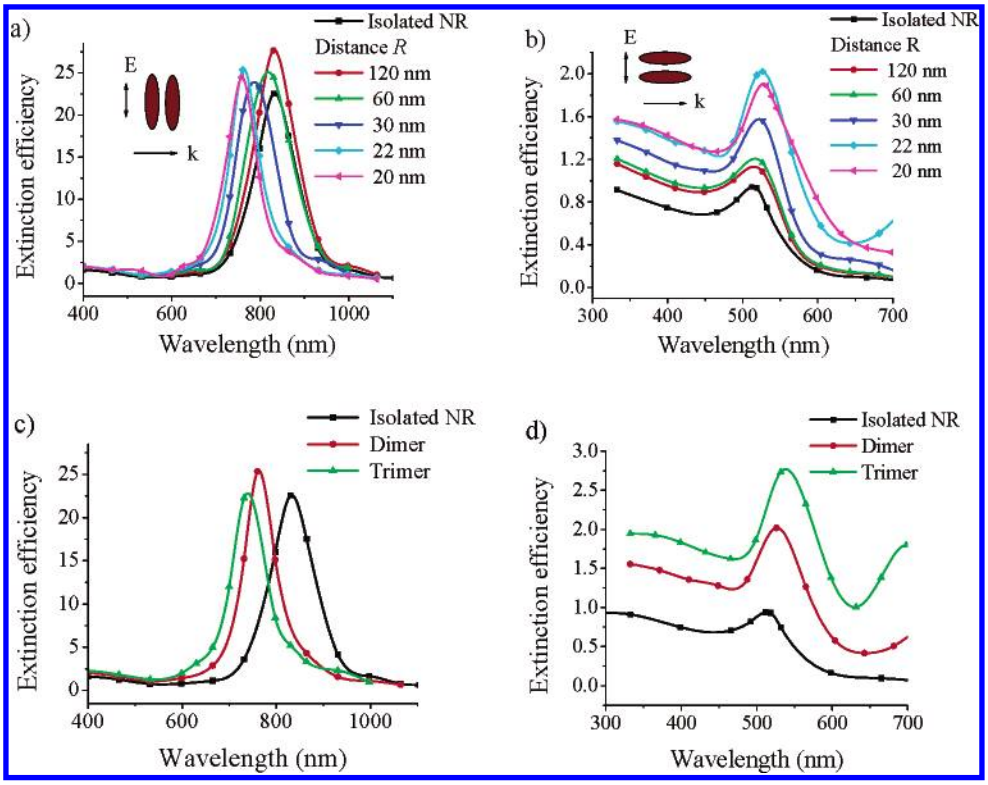

Figure 2. DDA-simulated extinction efficiency spectra of gold nanorods ($a \approx 80$ nm, $b \approx 20$ nm) assembled in a side-by-side orientation: (a) Longitudinal plasmon excitation and (b) transverse plasmon excitation of a pair of nanorods as a function of the internanorod center-to-center distance ($R = 120$, 60, 30, 22 nm and finally 20 nm where nanorods touch each other). The isolated nanorod spectrum is also shown as a black curve for comparison. (c) Longitudinal plasmon excitation and (d) transverse plasmon excitation of a nanorod assembly as a function of the number of nanorods (isolated nanorod, dimer and trimer) with the internanorod distance fixed at 22 nm.

assembly of nanorods most likely results from the electrostatic attraction between the positively charged nanorod surface and the negatively charged carboxylate ends of the citrate ions. The adsorbed citrate ions may either bridge between nanorods, or lead to the formation of local negatively charged regions on the nanorod that are electrostatically attracted to cationic regions on adjacent nanorods, or simply neutralize the electrostatic repulsion between the nanorods. Such a mechanism is expected to result predominantly in the side-by-side assembly of the gold nanorods.

Figure 1c shows examples of nanorods assembled side-by-side imaged by TEM. However, the TEM images are not entirely representative of the solution phase, due to the transfer of the sample to a planar solid support followed by evaporation of the solvent. The process of drying of a colloidal nanorod solution on the TEM grid itself has been studied by Nikoobakht et al.[68] and was found to result in the formation of side-by-side nanorod assemblies by the action of capillary forces. Such drying-mediated assemblies formed on the grids[86,87] cannot be distinguished from the assemblies formed in solution by the addition of the sodium citrate. Thus TEM, although a vital nanoparticle characterization tool, may not provide an accurate picture of solution phase behavior. Optical absorption measurements of the solution phase provide more definite characterization of the colloidal assembly process, especially when the interpretation of the experimental absorption results is aided by electrodynamic simulations of the optical spectra of model nanoparticle systems. We thus present electrodynamic simulations of the plasmon shift resulting from the assembly of nanorods for both side-by-side as well as end-to-end type assembly.

DDA Simulation of Nanorod Assembly. *Side-by-Side Assembly*. Figure 2a shows the DDA simulated optical spectra corresponding to the longitudinal plasmon excitation of a pair of gold nanorods, as they approach each other in a side-by-side orientation. The calculated longitudinal band of an isolated single nanorod ($AR = 4.0$) is shown for comparison as a black curve. When the nanorods are far apart ($R = 120$ nm), the optical resonance maximum does not seem to be shifted in position from that of the isolated nanorod case. As the nanorods approach each other, there is a clear blue-shift of the longitudinal plasmon band, as attributable to the coupling of the plasmons of the two interacting nanorods; the strength of this coupling increases with decreasing internanorod distance. The strength of coupling also increases with the number of nanorods interacting in an assembly. This is seen in Figure 2c from the larger blue-shift of the longitudinal plasmon band as we go from a nanorod dimer to a nanorod trimer. The effect of the side-by-side assembly on the transverse plasmon excitation (polarization direction along interparticle axis) has been similarly depicted in Figure 2b,d. In contrast to the longitudinal plasmon oscillation, the coupling of the transverse plasmon oscillations in side-by-side assembled nanorods leads to a red-shifted resonance. Thus the DDA simulation of the side-by-side nanorod assembly process agrees well with the experimental optical absorption band shifts induced by solution assembly/aggregation of nanorods in our experiments (Figure 1), confirming the side-by-side mechanism of nanorod assembly. Although 100% of the nanorods in our experimental sample may not be assembled in a perfect side-by-side orientation, the experimental optical spectra reflect the average characteristics of the colloidal assembly process in solution.

End-to-End Assembly. The calculated optical absorption spectra corresponding to the longitudinal plasmon excitation of a pair of gold nanorods, approaching each other along their long axis (i.e., end-to-end assembly) is shown in Figure 3a. The calculated longitudinal band of the isolated single nanorod ($AR = 4.0$) is shown for comparison as a black curve. The optical

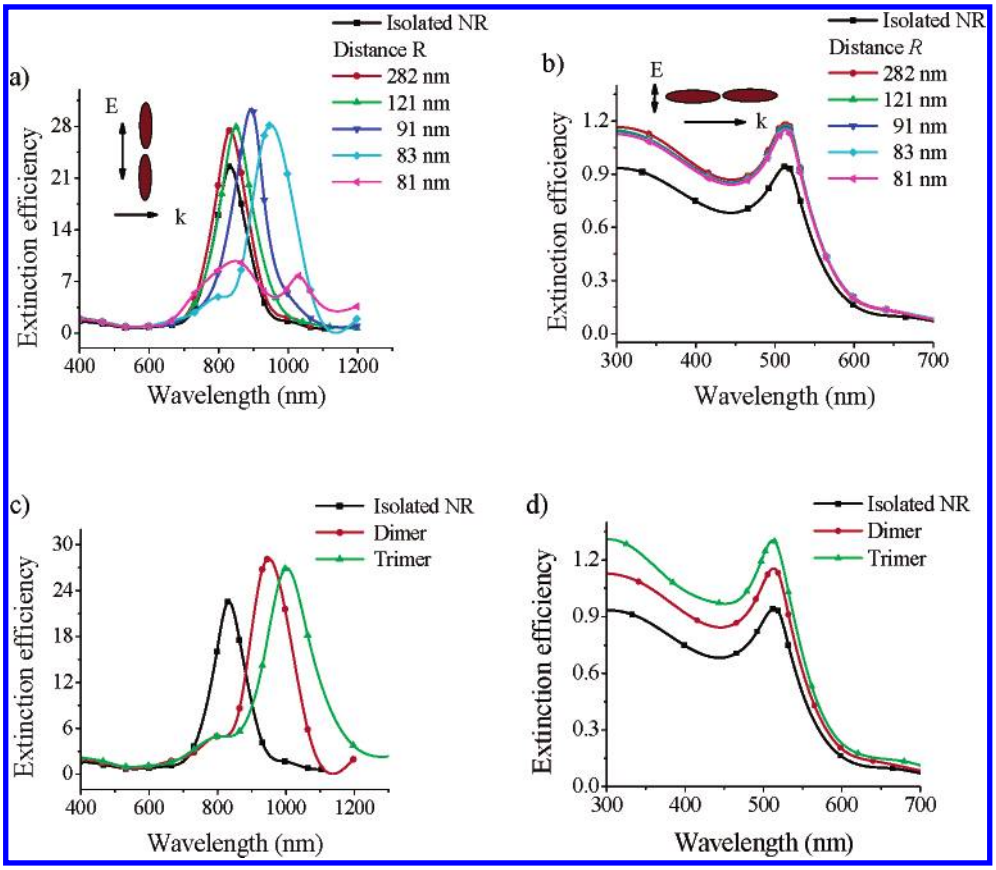

Figure 3. DDA-simulated extinction efficiency spectra of gold nanorods ($a \approx 80$ nm, $b \approx 20$ nm) assembled in an end-to-end orientation: (a) Longitudinal plasmon excitation and (b) transverse plasmon excitation of a pair of nanorods as a function of the internanorod center-to-center distance ($R = 282$, 121, 91, 83 nm and finally 81 nm where nanorods touch each other). The isolated nanorod spectrum is also shown as a black curve for comparison. (c) Longitudinal plasmon excitation and (d) transverse plasmon excitation of a nanorod assembly as a function of the number of nanorods (isolated nanorod, dimer, and trimer) with the internanorod distance fixed at 83 nm.

resonance maximum does not seem to shift its position from that of the isolated nanorod case for a large internanorod distance ($R = 282$ nm). As the distance decreases, the longitudinal plasmon band progressively red-shifts due to the coupling of the longitudinal plasmons. Figure 3c shows that as we go from a nanorod dimer to a nanorod trimer, there is a larger red-shift of the longitudinal plasmon band. Whereas the longitudinal plasmon band red-shifts, the transverse plasmon resonance does not show any appreciable shift for the end-to-end alignment (Figure 3b,d). These simulation results are in agreement with the experimental results of Kamat and co-workers[72] and Joseph et al.[73]

The anisotropic shape of nanorods thus allows two orientational modes of nanorod plasmon coupling, i.e., end-to-end and side-by-side. The DDA simulation results confirm the experimental suggestion that these two modes of coupling result in plasmon shifts in opposite directions. These results are also consistent with earlier theoretical predictions by Gluodenis et al.[82] of the spectral shifts resulting from the dipolar interaction of a pair of cylindrical gold nanoparticles as well as a recent investigation of the optical extinction characteristics of metal nanorod arrays by Cortie et al.[88]

Origin of Assembly Induced Plasmon Shift: Dipolar Exciton Coupling Model. Dimerization and aggregation in organic molecules and its effect on their optical absorption and fluorescence is very well studied.[76] The dipole−dipole interactions between individual chromophores/fluorophores in the aggregate are generally described in the framework of the exciton coupling theory.[74,75] Exciton theory predicts that the excited-state levels of the monomer split in two levels upon dimerization, a lower energy level and a higher energy level relative to the monomer excited state corresponding respectively to two possible arrangements of the transition dipoles of the chromophores in the dimer, i.e., in-phase or symmetric and out-of-phase or antisymmetric (see Figure 4). The energy splitting $2U$ is given by the interaction energy between the chromophores which is approximated by the Coulombic interaction between the transition dipole moments of the monomers, the angle and the distance between the transition dipoles, 1 and 2:[89]

$$U = \frac{1}{4\pi\epsilon_0 n_m^2 R^3} |\mu|^2 \kappa \qquad (1)$$

where $\kappa = \cos\theta_{12} - 3\cos\theta_{1R}\cos\theta_{2R}$ is the orientation factor, n_m is the refractive index of the medium, $|\mu|^2$ is the squared modulus of the transition dipole moment, and R is the distance between the dipole centers. Although transitions from the ground state to either excited state are possible, the number of spectral bands observed depends on the geometry of the dimer.[76,89,90] For parallel or *H*-type dimers (Figure 4a), transition to the lower energy excited state is forbidden due to the cancellation of the two dipole moments in this configuration and the spectrum consists of a single band at higher energy with respect to the monomer (because $\theta_{12} = 0°$, $\theta_{1R} = \theta_{1R} = 90°$, and so $\kappa_H = 1$) for which the interaction between the two transition dipoles of the dimer is repulsive. For head-to-tail or *J*-type dimers (Figure 4b), transition to the higher energy state is forbidden due to the cancellation of the two dipole moments in this configuration and the spectrum shows a single band at lower energy with

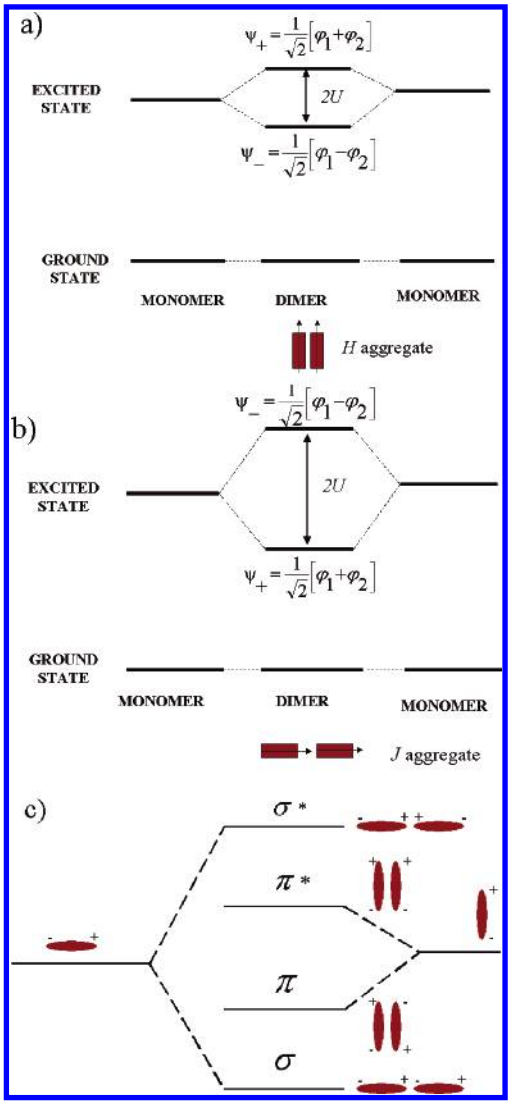

Figure 4. Schematic of the energy level splitting resulting from the dipolar interaction of chromophores in a dimer, showing symmetric (ψ_+) and antisymmetric coupling (ψ_-) of excitons for (a) *H* aggregate geometry and (b) *J* aggregate geometry. (c) Exciton theory picture of the nature of the coupled longitudinal plasmon excitation in nanorod dimers: electromagnetic analogy to molecular orbital theory.

respect to the monomer (because $\theta_{12} = \theta_{1R} = \theta_{1R} = 0°$ and so $\kappa_J = -2$) for which the interaction between dipoles is attractive.

By considering the nanorod plasmons to be effectively excitons, the exciton coupling theory can used to explain the optical spectra of the nanorod dimers. The side-by-side nanorod dimer, for the case of longitudinal polarization, represents an *H* aggregate and hence we observe a blue-shifted spectrum. Conversely, the end-to-end assembly is a *J* aggregate, resulting in a red-shifted spectrum. For the transverse polarization, the side-by-side nanorod arrangement is a *J* aggregate (provided the polarization direction is along the interparticle axis) leading to the red-shift and the end-to-end configuration is an *H* aggregate (however, the expected blue-shift of the transverse band may be too small to be observable because the transverse plasmon dipoles are far apart even when the rods touch each other). Thus, the optical properties of the gold nanorod assemblies and their dependence on the assembly orientation seem to be qualitatively consistent with the exciton-coupling model.

Similar reasoning also applies to the polarization dependence of the optical resonance shift in nanosphere dimers,[41] where a

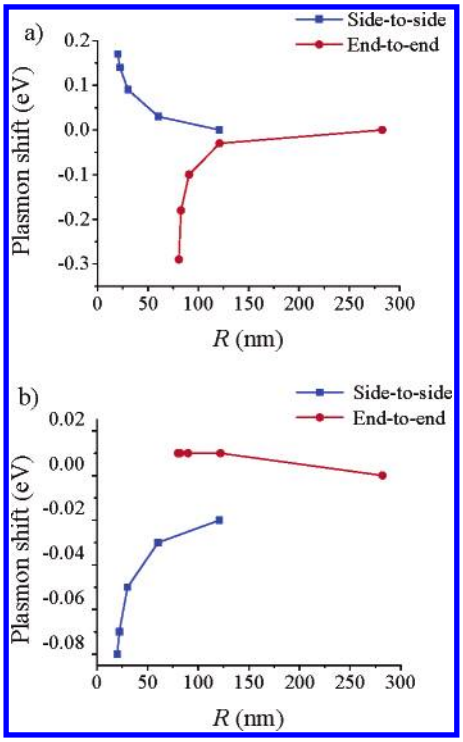

Figure 5. Energy shift of the surface plasmon resonance for side-by-side (blue squares) and end-to-end dimerization (red circles) of gold nanorods ($a \approx 80$ nm, $b \approx 20$ nm) as a function of the internanorod center-to-center distance *R* for (a) longitudinal plasmon and (b) transverse plasmon oscillation.

polarization along the interparticle axis (*p*-pol) results in a red-shift with respect to the single nanosphere resonance whereas a perpendicular polarization (*s*-pol) results in a blue-shift. (Supporting Information Figure S1) The near-infrared optical resonances of silica-gold core−shell particles can also be explained in terms of the exciton coupling between the plasmon supported on the outer surface of a gold sphere and that on the inner surface of a cavity.[91] In this case, the line along which the charges interact is parallel to the dipole moment vectors, corresponding to a *J*-type symmetry resulting in a bonding or symmetric resonance red-shifted with respect to the visible resonance of the solid gold nanosphere (around 520 nm). The antisymmetric coupling or antibonding resonance is also an allowed mode since the sphere and cavity plasmon dipole moments do not cancel out but is expected to be on the UV end of the spectrum.

Trends in Assembly Induced Plasmon Shift. The assembly induced plasmon shift, in energy units, gives a measure of the strength of interparticle plasmon coupling. Figure 5 shows the increasing trend of the plasmon energy shift with decreasing internanorod distance *R* for end-to-end and side-by-side nanorod dimers. There is qualitative agreement between the simulation results and exciton theory. As seen from Figure 5a, the magnitude of longitudinal plasmon shift for a given internanorod distance is larger for the case of end-to-end dimerization, which can possibly be reconciled with the greater strength of the *J*-type interaction ($|\kappa_J| > |\kappa_H|$). Similarly, the magnitude of transverse plasmon shift (Figure 5b) is larger for the side-by-side dimerization case. For the same symmetry (*H* or *J*), shifts of the longitudinal plasmon band can be seen to be more prominent than those of the transverse plasmon band, which may be explained in the context of the exciton model as being due to the greater oscillator strength of the longitudinal plasmon excitation (as also seen from the higher spectral intensity of

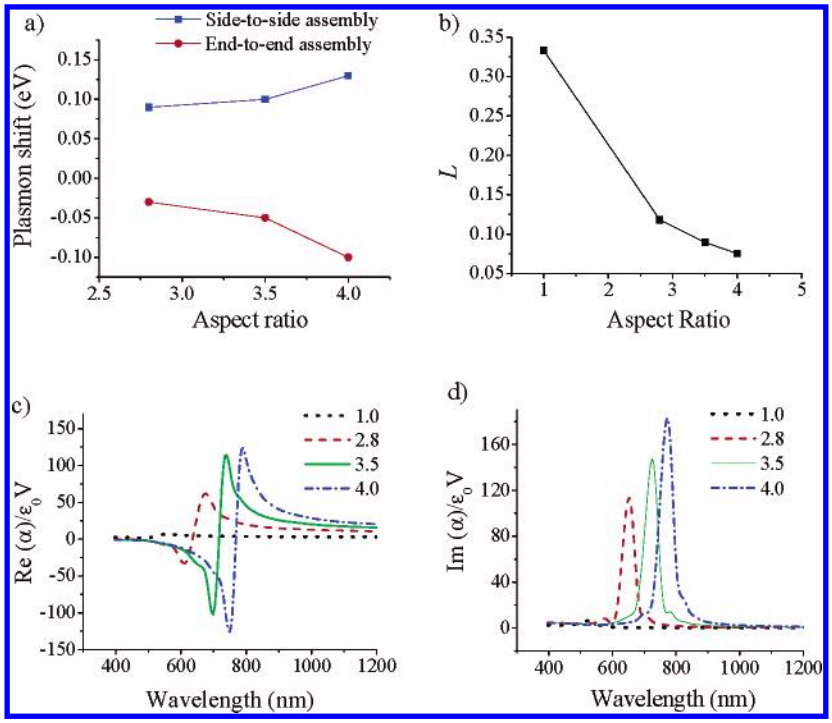

Figure 6. (a) Plot of the assembly induced plasmon energy shift (in eV) versus the nanorod aspect ratio *AR* for side-by-side (blue squares) and end-to-end dimerization (red dots). Values of the (b) nanorod depolarization factor *L*, (c) real part, and (d) imaginary part of the dipole polarizability, calculated for different aspect ratio values *AR* = 1.0 (sphere), 2.8, 3.5, and 4.0 on the basis of the Classius−Missotti equation. The medium refractive index n_m was set equal to 1.33.

the longitudinal plasmon band as compared to transverse plasmon band). This makes nanorods much more attractive as compared to nanospheres for analyte-sensing assays based on nanoparticle aggregation.[15] Note that the dependence of the plasmon energy shift with internanorod distance does not however correlate with the $1/R^3$ dependence predicted by the exciton model (Equation 1). This may be because the exciton-coupling model only considers interactions between point dipoles at relatively large inter-dipole distances; higher order multipole-multipole interactions are neglected in the weak interaction limit. On the other hand, each nanorod target in our electrodynamic simulation is represented by a few thousand dipoles while accounting for the finite particle size effects (e.g., electromagnetic retardation[78,92]) and the higher order interparticle interactions[43] (which become important in the strong coupling limit and/or very small interparticle distances). Besides, due to the finite size of the particles, the center-to-center distance *R* does not represent the distance at which the charges induced on neighboring particles interact.

Nature of the Coupled Plasmon Excitation: **Electromagnetic Analogy to Molecular Orbitals.** The effect of interparticle coupling on the nature of plasmon excitation and electric-field enhancement is expected to have important consequences for the use of nanorod assemblies in near-field-coupling based applications i.e., plasmon propagation[24−29] and field-enhanced spectroscopy.[92] The exciton model, in addition to the explanation of optical band shifts, also predicts the nature of the plasmon excitation in the coupled system (see Figure 4c). As suggested by the exciton model, the coupled longitudinal plasmon for the end-to-end dimer is bonding in nature analogous to the formation of a σ bond from two p_z orbitals. The resulting electric field intensity is maximum in the junction between the interacting nanorods. On the other hand, the coupled longitudinal plasmon for the side-by-side dimer has an antibonding nature analogous to the formation of a π^* bond from $p_{x/y}$ orbitals, with the electric field concentrated on either side of the interparticle junction. This contrast between the two modes of assembly is reinforced by the following observation. In the case of the end-to-end assembly simulation, a new band emerges at higher energies (attributable to higher-order interactions or image interactions[43]) as the internanorod distance becomes very small[93] (Figure 3a) or the number of nanorods interacting in an assembly increases (Figure 3c). The side-by-side assembly simulation does not show such an effect. The plasmons of closely spaced rods aligned end-to-end interact very strongly supporting an intense electric field at the interparticle junction, consistent with an earlier theoretical study on electromagnetic coupling in large gold nanorods by Aizpurua et al.[92]

Dependence of Plasmon Coupling Strength on Nanorod Aspect Ratio. The longitudinal plasmon spectra of the side-by-side and end-to-end dimers were calculated for three different aspect ratio values *AR* = 2.8, 3.5, and 4.0 (Supporting Information Figure S2). Note that the internanorod distance *R* was kept at a constant value for the three cases i.e., about 25 nm for side-by-side assembly and about 91 nm for end-to-end assembly. The nanorod effective radius (and hence the total number of gold atoms) was kept constant at r_{eff} = 16 nm. The plasmon energy shift is plotted against the nanorod aspect ratio in Figure 6a. For both side-by-side as well as end-to-end assembly, the strength of plasmon coupling as evidenced by the magnitude of the plasmon energy shift (in eV) is seen to increase with increasing nanorod aspect ratio in the selected range of investigation. In the context of exciton theory, this can be explained on the basis of an increase in the nanorod dipole polarizability α and hence the dipole moment μ with increasing nanorod aspect ratio. Elucidating further, the dipole moment of the nanorod plasmon in the quasi-static limit is given as:[82]

$$\mu = \epsilon_m \alpha \hat{E} \qquad (2)$$

where $\hat{E}$ is the electric field experienced by the nanorod and $\epsilon_m = n_m^2$ is the medium dielectric constant. As per the Classius−

Mossoti relation[54] for the polarizability corresponding to the longitudinal excitation:

$$\alpha = \frac{\epsilon_0 V}{L}\left(\frac{\epsilon - \epsilon_m}{\epsilon + \left(\frac{1-L}{L}\right)\epsilon_m}\right) \quad (3)$$

where V is the nanorod volume, ϵ_0 is the vacuum permittivity and $\epsilon = \epsilon_1 + i\epsilon_2$ is the complex dielectric function of gold. L is the depolarization factor corresponding to the long-axis and can be expressed as a function of the nanorod aspect ratio AR as:[56,82]

$$L = \frac{1-e^2}{e^2}\left(\frac{1}{2e}\ln\frac{1+e}{1-e} - 1\right) \quad (4)$$

$$e = \sqrt{1-(1/AR)^2} \quad (5)$$

The value of L is 1/3 for a sphere and decreases with increasing nanorod aspect ratio (Figure 6b). The resonance condition from eq 2 is given by:

$$\epsilon_1 = -\left(\frac{1-L}{L}\right)\epsilon_m \quad (6)$$

This is provided ϵ_2 is small or weakly dependent on frequency,[54] which is valid in the 600−850 nm region for gold.[83] Equation 6 explains the red-shift of the longitudinal plasmon resonance with increasing aspect ratio since the negative real part of the dielectric function ϵ_1 for gold increases with increasing wavelength.[83] At resonance, α is given as:

$$\mathrm{Re}(\alpha) = \frac{\epsilon_0 V}{L} \quad (7)$$

$$\mathrm{Im}(\alpha) = \frac{\epsilon_0 V}{L^2}\left(\frac{\epsilon_m}{\epsilon_2}\right) \quad (8)$$

The rapid decrease in L with increasing aspect ratio against a slight increase in the imaginary part of the dielectric constant with wavelength (in the region of investigation) predicts a larger polarizability for higher aspect ratios. This is depicted in the calculated plots of the real and imaginary parts of the nanorod dipole polarizability for the different aspect ratio values (Figure 6c,d). The explanation of increasing plasmon coupling strength with increasing nanorod aspect ratio on the basis of the quasistatic and dipole approximations serves only as a qualitative one since finite particle size (as compared to the wavelength of light) effects[78,92] and higher order interactions[43] are not included.

Symmetry-Breaking in Heterodimers. The calculated longitudinal plasmon spectrum for a dimer with two nanorods having dissimilar aspect ratios (AR = 2.8 and 4.0, respectively) but the same width ($b \approx 21$ nm) is shown for the side-by-side case in Figure 7a. As seen from Figure 7a, the longitudinal plasmon maximum is around 695 nm for an isolated nanorod of aspect ratio 2.8 and around 835 nm for an isolated nanorod of aspect ratio 4.0. However, plasmon coupling in the assembled dimer results in a spectrum with a blue-shifted component around 680 nm (corresponding to the symmetric plasmon coupling mode) and a red-shifted component around 930 nm (corresponding to the antisymmetric coupling mode). For a side-by-side dimer with rods of the same length, the antisymmetric coupling mode with lower energy would have a zero dipole moment and absorption to that level will not be observed optically. However, when the rod lengths are dissimilar,

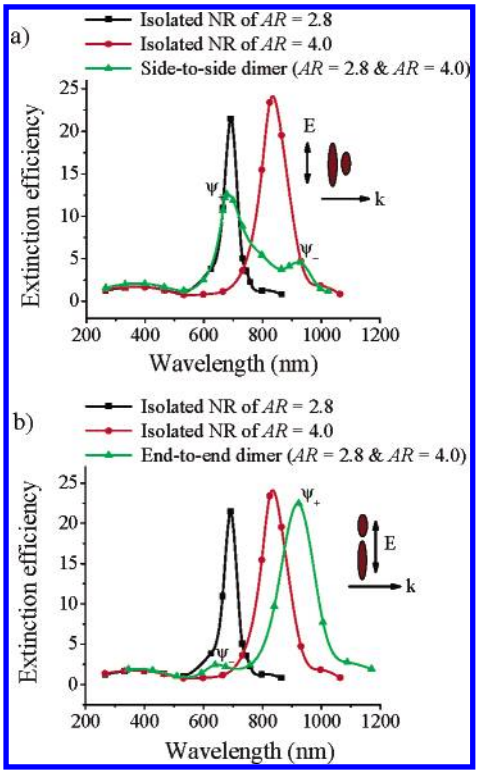

Figure 7. DDA-simulated extinction efficiency spectrum (corresponding to the longitudinal plasmon excitation) of a dimer of nanorods of dissimilar aspect ratios (AR = 2.8 and 4.0, respectively) but the same width ($b \approx 21$ nm), (a) interacting side-by-side with internanorod distance R = 21 nm where nanorods touch each other and (b) interacting end-to-end with internanorod distance R = 70 nm where nanorods touch each other. Calculated spectra of the isolated nanorods are also shown for comparison.

absorption to this red-shifted level becomes observed, although it possesses a lower spectral intensity due to the lower net dipole moment. The transverse band on assembly shows a single blue-shifted band around 505 nm (data not shown), which is expected since the two nanorods irrespective of their aspect ratios have the same transverse plasmon oscillation energy. Similarly as shown in Figure 7b, when rods of dissimilar aspect ratio are assembled end-to-end, the higher energy component corresponding to the antisymmetric coupling becomes allowed due to symmetry breaking, although it possesses a relatively lower spectral intensity. Experimental realization of this symmetry breaking is rendered difficult due to the heterogeneous nature of the colloidal assembly process and the broad spectral bandwidths of the nanorod solutions.

The calculated spectra of rod-sphere dimers interacting side-by-side as well as end-to-end (with the light polarization along the nanorod long-axis) are seen to be red-shifted with respect to the isolated nanorod resonance (Supporting Information Figure S3). This can be explained on similar grounds as being due to the coupling of the nanorod longitudinal plasmon oscillation and the nanosphere oscillation. The magnitude of the shift for rod-sphere pairs is relatively smaller than in the case of nanorod pairs due to the energy mismatch between the longitudinal plasmon and the transverse plasmon modes and the weaker oscillator strength of the transverse plasmon mode. The blue-shifted component corresponding to the nanosphere resonance is too weak in intensity to be identified.

Dependence of Plasmon Coupling on the Angle between the Nanorod Axes. The angle between the long axes of two nanorods assembled side-by-side was varied as $\theta_{12} = 0$, 45, and

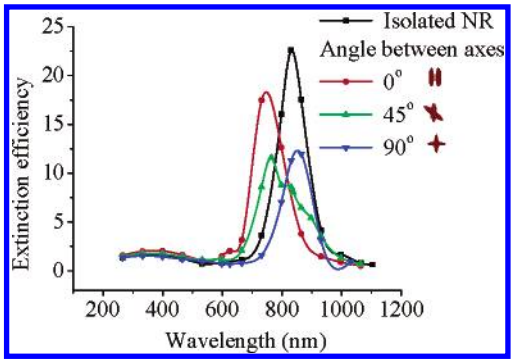

Figure 8. DDA-simulated extinction efficiency spectra of a dimer of gold nanorods assembled side-by-side (internanorod distance $R = 20$ nm, i.e., nanorods touching each other) as a function of the angle between the long-axes of the nanorod. The light polarization direction was maintained along one of the nanorods. The spectrum of the isolated nanorod is shown as a black curve for comparison.

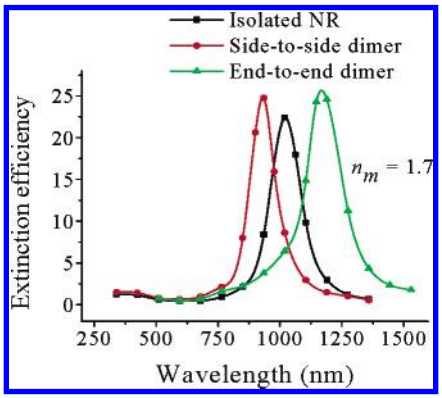

Figure 9. DDA-simulated extinction efficiency spectra (corresponding to the longitudinal plasmon excitation) of a dimer of gold nanorods interacting side-by-side (shown in blue) with internanorod distance $R = 22$ nm and end-to-end (shown in red) with internanorod distance $R = 83$ nm for medium refractive index $n_m = 1.7$. The spectrum of the isolated nanorod (black curve) is shown for comparison.

90° with the light polarization along the long-axis of one of the nanorods. The simulated spectra have been shown for the three cases in Figure 8. For the case of 0°, i.e., with the dipoles aligned parallel to each other, the maximum blue-shift can be seen (corresponding to $\kappa = 1$). On the other hand, at an angle of 90° between the plasmons (corresponding to $\kappa = 0$), no spectral blue-shift is seen, i.e., the longitudinal plasmons do not couple. A slight red-shift is observed due to the coupling of the longitudinal plasmon of one nanorod with the transverse plasmon of the other nanorod. At an angle of 45° (corresponding to $\kappa = 1/\sqrt{2}$), a plasmon blue-shift is seen, the extent of shift slightly smaller compared to the case of $\theta_{12} = 0°$ or parallel alignment. A red-shifted component is also seen as a combined effect of the antisymmetric coupling of the interacting plasmons (nonzero sum of dipole moments) in combination with the coupling of the longitudinal plasmon of one nanorod to the transverse plasmon mode of another.

Dependence of Plasmon Coupling on the Surrounding Medium. The $1/n_m^2$ dependence of the interaction energy in the exciton-coupling model (eq 1) predicts the interparticle plasmon interaction to be shielded by the medium dielectric. Figure 9 shows the calculated longitudinal plasmon resonance of side-by-side and end-to-end assembled nanorod dimers with respect to the isolated single nanorod resonance, in a medium of refractive index $n_m = 1.7$. Equation 6 explains the red-shift of the single nanorod resonance with increase in the medium refractive index n_m. By comparison with the case of $n_m = 1.33$ for a similar internanorod distance, it can be seen that the increase in the medium refractive index to $n_m = 1.7$ results in a small decrease in the magnitude of the plasmon shift (0.03 eV for side-by-side dimerization and 0.01 eV for end-to-end dimerization). However, any dependence of the interparticle plasmon coupling on the medium refractive index is however complicated by the fact that increase in n_m results in the red-shift of λ_m, increase in the nanorod polarizability (eq 8) and dipole moment (eq 2) and the variation in finite-particle size effects and multipolar contributions.

IV. Conclusions

Electrodynamic simulations of nanoparticle systems based on the DDA method provide a solid basis for the interpretation of experimental optical spectra as well as apriori prediction of the trends in optical properties. In our experiments, we observed that the solution assembly of nanorods induced by the addition of sodium citrate resulted in the blue-shift of the longitudinal nanorod plasmon band—an observation in contrast to the red-shift observed in earlier studies[72,73] involving the end-to-end assembly of nanorods. The analysis of the assembly mechanism in our experiments pointed toward a side-by-side assembly of nanorods in solution; confirmation was obtained from the agreement of DDA simulations of dimers of nanorods with the observed plasmon shifts. Assembly induced plasmon shift results from internanorod plasmon coupling, the strength of which was seen from the simulation results to increase with a decrease in the internanorod distance, an increase in the number of interacting nanorods and an increase in the nanorod aspect ratio for both side-by-side as well as end-to-end assembly. Most qualitative features of the simulated trends in interparticle plasmon coupling could be explained by treating the plasmon oscillation as an exciton. On the basis of the exciton theory, an analogy could be drawn between the orientational modes of nanorod assembly and the well-known *H* and *J* aggregation of organic chromophores. However, quantitative deviations from the exciton theory arise as a result of the multidipolar nature of the plasmonic interaction and the effect of finite particle size. An additional interesting theoretical observation was the symmetry breaking in dimers of nanorods either having dissimilar aspect ratios or oriented nonparallel to each other, which resulted in longitudinal plasmon resonance with both a blue-shifted and a red-shifted band. The coupled nanorod plasmons can also thought of as electromagnetic analogues of molecular orbitals. The strong contrast between the bonding nature of the end-to-end nanorod plasmon coupling and the antibonding nature of the side-by-side coupling is manifested in optical spectra of the assemblies; the effect of this contrast on field enhancement-based properties needs to be exploited further.

Acknowledgment. This work is supported by the Materials Research Division of the National Science Foundation (# 0138391). Computations were supported by the Center for Computational Molecular Science and Technology at Georgia Tech and partially funded through a Shared University Research (SUR) grant from IBM and Georgia Tech. We thank the Center for Nanostructure Characterization and Fabrication at Georgia Tech for use of their Transmission Electron Microscopy facilities. We thank B. T. Draine and P. J. Flatau for use of their DDA code, DDSCAT 6.1, and Dr. K. S. Lee for setting up the DDSCAT program.

Supporting Information Available: DDA-simulated extinction efficiency spectra of (1) nanosphere dimer under *p*- and *s*-

polarizations, (2) nanorod dimer for different aspect ratios ($AR = 2.8$, 3.5 and 4.0), and (3) rod-sphere dimer for side-to-side and end-to-end assembly. This material is available free of charge via the Internet at http://pubs.acs.org.

References and Notes

(1) Mann, S.; Shenton, W.; Li, M.; Connolly, S.; Fitzmaurice, D. *Adv. Mater. (Weinheim, Ger.)* **2000**, *12*, 147.

(2) Mirkin, C. A. *Inorg. Chem.* **2000**, *39*, 2258.

(3) Murphy, C. J.; Sau, T. K.; Gole, A. M.; Orendorff, C. J.; Gao, J.; Gou, L.; Hunyadi, S. E.; Li, T. *J. Phys. Chem. B* **2005**, *109*, 13857.

(4) Pileni, M. P. *J. Phys. Chem. B* **2001**, *105*, 3358.

(5) Pileni, M. P. *Appl. Surface Sci.* **2001**, *171*, 1.

(6) Pileni, M. P. *J. Phys.: Condens. Matter* **2006**, *18*, S67.

(7) Pileni, M. P.; Lalatonne, Y.; Ingert, D.; Lisiecki, I.; Courty, A. *Faraday Discuss.* **2003**, *125*, 251.

(8) Storhoff, J. J.; Mirkin, C. A. *Chem. Rev. (Washington, D. C.)* **1999**, *99*, 1849.

(9) Teranishi, T.; Miyake, M. *Encycl. Nanosci. Nanotechnol.* **2004**, *5*, 421.

(10) Davis, S. A.; Breulmann, M.; Rhodes, K. H.; Zhang, B.; Mann, S. *Chem. Mater.* **2001**, *13*, 3218.

(11) Alivisatos, A. P.; Johnsson, K. P.; Peng, X.; Wilson, T. E.; Loweth, C. J.; Bruchez, M. P., Jr.; Schultz, P. G. *Nature (London)* **1996**, *382*, 609.

(12) Mirkin, C. A.; Letsinger, R. L.; Mucic, R. C.; Storhoff, J. J. *Nature (London)* **1996**, *382*, 607.

(13) Alivisatos, P. *Nat. Biotechnol.* **2004**, *22*, 47.

(14) Shenton, W.; Davis, S. A.; Mann, S. *Adv. Mater. (Weinheim, Ger.)* **1999**, *11*, 449.

(15) Sudeep, P. K.; Joseph, S. T. S.; Thomas, K. G. *J. Am. Chem. Soc.* **2005**, *127*, 6516.

(16) Elghanian, R.; Storhoff, J. J.; Mucic, R. C.; Letsinger, R. L.; Mirkin, C. A. *Science (Washington, D. C.)* **1997**, *277*, 1078.

(17) Ando, M.; Kawasaki, M.; Imazeki, S.; Sasaki, H.; Kamata, T. *Appl. Phys. Lett.* **2004**, *85*, 1849.

(18) Feldheim, D. L.; Foss, C. A., Jr. *Met. Nanopart.* **2002**, 1.

(19) Hu, M.-S.; Chen, H.-L.; Shen, C.-H.; Hong, L.-S.; Huang, B.-R.; Chen, K.-H.; Chen, L.-C. *Nat. Mater.* **2006**, *5*, 102.

(20) Jin, Y.; Friedman, N. *J. Am. Chem. Soc.* **2005**, *127*, 11902.

(21) Maheshwari, V.; Saraf, R. F. *Science (Washington, D. C.)* **2006**, *312*, 1501.

(22) Tan, Y.; Li, Y.; Zhu, D. *Encyclo. Nanosci. Nanotechnol.* **2004**, *8*, 9.

(23) Pillai, S.; Catchpole, K. R.; Trupke, T.; Zhang, G.; Zhao, J.; Green, M. A. *Appl. Phys. Lett.* **2006**, *88*, 161102/1.

(24) Krenn, J. R.; Salerno, M.; Felidj, N.; Lamprecht, B.; Schider, G.; Leitner, A.; Aussenegg, F. R.; Weeber, J. C.; Dereux, A.; Goudonnet, J. P. *J. Microsc. (Oxford)* **2001**, *202*, 122.

(25) Maier, S. A.; Atwater, H. A. *J. Appl. Phys.* **2005**, *98*, 011101/1.

(26) Maier, S. A.; Brongersma, M. L.; Kik, P. G.; Meltzer, S.; Requicha, A. A. G.; Atwater, H. A. *Adv. Mater. (Weinheim, Ger.)* **2001**, *13*, 1501.

(27) Maier, S. A.; Friedman, M. D.; Barclay, P. E.; Painter, O. *Appl. Phys. Lett.* **2005**, *86*, 071103/1.

(28) Maier, S. A.; Kik, P. G.; Atwater, H. A.; Meltzer, S.; Harel, E.; Koel, B. E.; Requicha, A. A. G. *Nat. Mater.* **2003**, *2*, 229.

(29) Quinten, M.; Leitner, A.; Krenn, J. R.; Aussenegg, F. R. *Opt. Lett.* **1998**, *23*, 1331.

(30) Barnes, W. L.; Dereux, A.; Ebbesen, T. W. *Nature (London)* **2003**, *424*, 824.

(31) Feldstein, M. J.; Keating, C. D.; Liau, Y.-H.; Natan, M. J.; Scherer, N. F. *J. Am. Chem. Soc.* **1997**, *119*, 6638.

(32) Seker, F.; Malenfant, P. R. L.; Larsen, M.; Alizadeh, A.; Conway, K.; Kulkarni, A. M.; Goddard, G.; Garaas, R. *Adv. Mater. (Weinheim, Ger.)* **2005**, *17*, 1941.

(33) Liz-Marzan, L. M. *Langmuir* **2006**, *22*, 32.

(34) Grant, C. D.; Schwartzberg, A. M.; Norman, T. J., Jr.; Zhang, J. Z. *J. Am. Chem. Soc.* **2003**, *125*, 549.

(35) Lazarides, A. A.; Schatz, G. C. *J. Phys. Chem. B* **2000**, *104*, 460.

(36) Lin, S.; Li, M.; Dujardin, E.; Girard, C.; Mann, S. *Adv. Mater. (Weinheim, Ger.)* **2005**, *17*, 2553.

(37) Jain, P. K.; Qian, W.; El-Sayed, M. A. *J. Phys. Chem. B* **2006**, *110*, 136.

(38) Storhoff, J. J.; Lazarides, A. A.; Mucic, R. C.; Mirkin, C. A.; Letsinger, R. L.; Schatz, G. C. *J. Am. Chem. Soc.* **2000**, *122*, 4640.

(39) Su, K. H.; Wei, Q. H.; Zhang, X.; Mock, J. J.; Smith, D. R.; Schultz, S. *Nano Lett.* **2003**, *3*, 1087.

(40) Soennichsen, C.; Reinhard, B. M.; Liphardt, J.; Alivisatos, A. P. *Nat. Biotechnol.* **2005**, *23*, 741.

(41) Rechberger, W.; Hohenau, A.; Leitner, A.; Krenn, J. R.; Lamprecht, B.; Aussenegg, F. R. *Opt. Commun.* **2003**, *220*, 137.

(42) Nordlander, P.; Oubre, C.; Prodan, E.; Li, K.; Stockman, M. I. *Nano Lett.* **2004**, *4*, 899.

(43) Xiao, J. J.; Huang, J. P.; Yu, K. W. *Phys. Rev. B: Condens. Matter Mater. Phys.* **2005**, *71*, 045404/1.

(44) Haynes, C. L.; McFarland, A. D.; Zhao, L.; Van Duyne, R. P.; Schatz, G. C.; Gunnarsson, L.; Prikulis, J.; Kasemo, B.; Kaell, M. *J. Phys. Chem. B* **2003**, *107*, 7337.

(45) Sweatlock, L. A.; Maier, S. A.; Atwater, H. A.; Penninkhof, J. J.; Polman, A. *Phys. Rev. B: Condens. Matter Mater. Phys.* **2005**, *71*, 235408/1.

(46) Hao, E.; Schatz George, C. *J. Chem. Phys.* **2004**, *120*, 357.

(47) Jiang, J.; Bosnick, K.; Maillard, M.; Brus, L. *J. Phys. Chem. B* **2003**, *107*, 9964.

(48) Michaels, A. M.; Jiang, J.; Brus, L. *J. Phys. Chem. B* **2000**, *104*, 11965.

(49) Ritchie, G.; Burstein, E. *Phys. Rev. B: Condens. Matter Mater. Phys.* **1981**, *24*, 4843.

(50) Maillard, M.; Monchicourt, P.; Pileni, M. P. *Chem. Phys. Lett.* **2003**, *380*, 704.

(51) Shalaev, V. M.; Poliakov, E. Y.; Markel, V. A. *Phys. Rev. B: Condens. Matter Mater. Phys.* **1996**, *53*, 2437.

(52) Markel, V. A.; Shalaev, V. M.; Zhang, P.; Huynh, W.; Tay, L.; Haslett, T. L.; Moskovits, M. *Phys. Rev. B: Condens. Matter Mater. Phys.* **1999**, *59*, 10903.

(53) Link, S.; El-Sayed, M. A. *J. Phys. Chem. B* **1999**, *103*, 8410.

(54) Kreibig, U.; Vollmer, M. *Optical Properties of Metal Clusters*, Series in Materials Science 25; Springer: New York, 1995.

(55) Gans, R. *Ann. Phys. (Berlin)* **1915**, *47*, 270.

(56) Link, S.; Mohamed, M. B.; El-Sayed, M. A. *J. Phys. Chem. B* **1999**, *103*, 3073.

(57) Link, S.; El-Sayed, M. A.; Mohamed, M. B. *J. Phys. Chem. B* **2005**, *109*, 10531.

(58) Jain, P. K.; Lee, K. S.; El-Sayed, I. H.; El-Sayed, M. A. *J. Phys. Chem. B* **2006**, *110*, 7238.

(59) Gans, R. V. *Ann. Phys. (Berlin)* **1912**, *37*, 881.

(60) Mohamed, M. B.; Volkov, V.; Link, S.; El-Sayed, M. A. *Chem. Phys. Lett.* **2000**, *317*, 517.

(61) Eustis, S.; El-Sayed, M. *J. Phys. Chem. B* **2005**, *109*, 16350.

(62) Nikoobakht, B.; El-Sayed, M. A. *J. Phys. Chem. A* **2003**, *107*, 3372.

(63) Nikoobakht, B.; Wang, J. P.; El-Sayed, M. A. *Chem. Phys. Lett.* **2002**, *366*, 17.

(64) Dickson, R. M.; Lyon, L. A. *J. Phys. Chem. B* **2000**, *104*, 6095.

(65) Murphy, C. J.; Jana, N. R.; Gearheart, L. A.; Obare, S. O.; Caswell, K. K.; Mann, S.; Johnson, C. J.; Davis, S. A.; Dujardin, E.; Edler, K. J. *Chem. Nanomater.* **2004**, *1*, 285.

(66) Orendorff, C. J.; Hankins, P. L.; Murphy, C. J. *Langmuir* **2005**, *21*, 2022.

(67) Jana, N. R.; Gearheart, L. A.; Obare, S. O.; Johnson, C. J.; Edler, K. J.; Mann, S.; Murphy, C. J. *J. Mater. Chem.* **2002**, *12*, 2909.

(68) Nikoobakht, B.; Wang, Z. L.; El-Sayed, M. A. *J. Phys. Chem. B* **2000**, *104*, 8635.

(69) Gole, A.; Murphy, C. J. *Langmuir* **2005**, *21*, 10756.

(70) Caswell, K. K.; Wilson, J. N.; Bunz, U. H. F.; Murphy, C. J. *J. Am. Chem. Soc.* **2003**, *125*, 13914.

(71) Dujardin, E.; Mann, S.; Hsin, L.-B.; Wang, C. R. C. *Chem. Commun. (Cambridge)* **2001**, 1264.

(72) Thomas, K. G.; Barazzouk, S.; Ipe, B. I.; Joseph, S. T. S.; Kamat, P. V. *J. Phys. Chem. B* **2004**, *108*, 13066.

(73) Joseph, S. T. S.; Ipe, B. I.; Pramod, P.; Thomas, K. G. *J. Phys. Chem. B* **2006**, *110*, 150.

(74) Kasha, M. *Radiat. Res.* **1963**, *20*, 55.

(75) Kasha, M.; Rawls, H. R.; El-Bayoumi, M. A. *Pure Appl. Chem.* **1965**, *11*, 371.

(76) Valdes-Aguilera, O.; Neckers, D. C. *Acc. Chem. Res.* **1989**, *22*, 171.

(77) Draine, B. T.; Flatau, P. J. *J. Opt. Soc. Am. A* **1994**, *11*, 1491.

(78) Kelly, K. L.; Coronado, E.; Zhao, L. L.; Schatz, G. C. *J. Phys. Chem. B* **2003**, *107*, 668.

(79) Schatz, G. C. *Theochem* **2001**, *573*, 73.

(80) Brioude, A.; Jiang, X. C.; Pileni, M. P. *J. Phys. Chem. B* **2005**, *109*, 13138.

(81) Lee, K.-S.; El-Sayed, M. A. *J. Phys. Chem. B* **2005**, *109*, 20331.

(82) Gluodenis, M.; Foss, C. A., Jr. *J. Phys. Chem. B* **2002**, *106*, 9484.

(83) Johnson, P. B.; Christy, R. W. *Phys. Rev. B: Condens. Matter Mater. Phys.* **1972**, *6*, 4370.

(84) Draine, B. T.; Goodman, J. *Astrophys. J.* **1993**, *405*, 685.

(85) Eustis, S.; El-Sayed, M. A. *J. Appl. Phys.* 2006, in press.

(86) Taleb, A.; Petit, C.; Pileni, M. P. *Chem. Mater.* **1997**, *9*, 950.

(87) Motte, L.; Billoudet, F.; Lacaze, E.; Douin, J.; Pileni, M. P. *J. Phys. Chem. B* **1997**, *101*, 138.

(88) Cortie, M. B.; Xu, X.; Ford, M. J. *Phys. Chem. Chem. Phys.* **2006**, *8*, 3520.

(89) Packard, B. Z.; Toptygin, D. D.; Komoriya, A.; Brand, L. *J. Phys. Chem. B* **1998**, *102*, 752.

(90) Kasha, M. *Phys. Process. Radiation Biol., Proc. Intern. Symp., Mich. State Univ.* **1964**, 17.

(91) Prodan, E.; Radloff, C.; Halas, N. J.; Nordlander, P. *Science (Washington, D. C.)* **2003**, *302*, 419.

(92) Aizpurua, J.; Bryant, G. W.; Richter, L. J.; Garcia de Abajo, F. J.; Kelley, B. K.; Mallouk, T. *Phys. Rev. B: Condens. Matter Mater. Phys.* **2005**, *71*, 235420/1.

(93) The spectral band structure is significantly altered when the two nanorods are touching each other end-to-end (Figure 5a, $R = 81$ nm). Interesting spectral characteristics of particles touching each other have already been investigated by Atwater and co-workers (ref 45). At the same time, exceptions to the applicability of electrodynamic simulations to particles touching each other have also been cited (ref 46).